
AFRL-RY-WP-TP-2023-0265

# A GENERALIZED GAMMA COPULA MODEL FOR HIGH RESOLUTION POLARIMETIC SAR CHANGE DETECTION (Preprint)

**Stephen Herman and Joshua Ash**
**Wright State University**

**NOVEMBER 2023**
**Final Report**



**AIR FORCE RESEARCH LABORATORY**
**SENSORS DIRECTORATE**
**WRIGHT-PATTERSON AIR FORCE BASE, OH 45433-7320**
**AIR FORCE MATERIEL COMMAND**
**UNITED STATES AIR FORCE**

# REPORT DOCUMENTATION PAGE

**PLEASE DO NOT RETURN YOUR FORM TO THE ABOVE ORGANIZATION.**

| 1. REPORT DATE | 2. REPORT TYPE | 3. DATES COVERED | |
|---|---|---|---|
| | | START DATE | END DATE |
| November 2023 | Conference Paper Preprint | 30 October 2023 | 30 October 2023 |

**4. TITLE AND SUBTITLE**

A GENERALIZED GAMMA COPULA MODEL FOR HIGH RESOLUTION POLARIMETIC SAR CHANGE DETECTION (Preprint)

| 5a. CONTRACT NUMBER | 5b. GRANT NUMBER | 5c. PROGRAM ELEMENT NUMBER |
|---|---|---|
| N/A | N/A | N/A |
| **5d. PROJECT NUMBER** | **5e. TASK NUMBER** | **5f. WORK UNIT NUMBER** |
| N/A | N/A | N/A |


**6. AUTHOR(S)**

Stephen Herman and Joshua Ash

**7. PERFORMING ORGANIZATION NAME(S) AND ADDRESS(ES)**

Wright State University
3640 Colonel Glenn Hwy,
Dayton, OH 45435


**8. PERFORMING ORGANIZATION REPORT NUMBER**

| 9. SPONSORING/MONITORING AGENCY NAME(S) AND ADDRESS(ES) | 10. SPONSOR/MONITOR'S ACRONYM(S) | 11. SPONSOR/MONITOR'SREPORT NUMBER(S) |
|---|---|---|
| Air Force Research Laboratory<br>Sensors Directorate<br>Wright-Patterson Air Force Base, OH 45433-7320<br>Air Force Materiel Command<br>United States Air Force | AFRL/RYDR | AFRL-RY-WP-TP-2023-0265 |

**12. DISTRIBUTION/AVAILABILITY STATEMENT**

DISTRIBUTION STATEMENT A. Approved for public release; distribution is unlimited.

**13. SUPPLEMENTARY NOTES**


PAO case number AFRL-2023-5422, Clearance Date 30 October 23. This work was funded in whole or in part by Department of the Air Force. The U.S. Government has for itself and others acting on its behalf an unlimited, paid-up, nonexclusive, irrevocable worldwide license to use, modify, reproduce, release, perform, display, or disclose the work by or on behalf of the U. S. Government. Report contains color.


**14. ABSTRACT**


In this paper, we describe a new approach to non-coherent change detection for high resolution polarimetric synthetic aperture radar (polSAR) exploitation. In the high resolution setting, the reduced size of a resolution cell diminishes the applicability of central limit theorem arguments that lead to the traditional Gaussian backscatter models that underpin existing polSAR change detection algorithms. To mitigate this, we introduce a new model for polSAR data that combines generalized Gamma (GG) distributed marginals within a copula framework to capture the correlation dependency between multiple polSAR channels. Using the GG-copula model, a generalized likelihood ratio test (GLRT) is derived for detecting changes within high resolution polSAR imagery. Examples using measured data demonstrate the non-Gaussian nature of high resolution polSAR data and quantify significant performance improvement when using the proposed GG-copula change detection framework.



**15. SUBJECT TERMS**

synthetic aperture radar, polarimetry, change detection, copulas, interferometric SAR, radar imaging, detection


| 16. SECURITY CLASSIFICATION OF: | | | 17. LIMITATION OF ABSTRACT | 18. NUMBER OF PAGES |
|---|---|---|---|---|
| a. REPORT | b. ABSTRACT | C. THIS PAGE | | |
| Unclassified | Unclassified | Unclassified | SAR | 8 |

| 19a. NAME OF RESPONSIBLE PERSON | 19b. PHONE NUMBER *(Include area code)* |
|---|---|
| Andrew Duly | N/A |

# A Generalized Gamma Copula Model for High Resolution Polarimetric SAR Change Detection

Stephen Herman
*Department of Electrical Engineering*
*Wright State University*
Dayton OH, USA

Joshua Ash
*Department of Electrical Engineering*
*Wright State University*
Dayton OH, USA

***Abstract*—In this paper, we describe a new approach to non-coherent change detection for high resolution polarimetric synthetic aperture radar (polSAR) exploitation. In the high resolution setting, the reduced size of a resolution cell diminishes the applicability of central limit theorem arguments that lead to the traditional Gaussian backscatter models that underpin existing polSAR change detection algorithms. To mitigate this, we introduce a new model for polSAR data that combines generalized Gamma ($G\Gamma$) distributed marginals within a copula framework to capture the correlation dependency between multiple polSAR channels. Using the $G\Gamma$-copula model, a generalized likelihood ratio test (GLRT) is derived for detecting changes within high resolution polSAR imagery. Examples using measured data demonstrate the non-Gaussian nature of high resolution polSAR data and quantify significant performance improvement when using the proposed $G\Gamma$-copula change detection framework.**

***Index Terms*—Synthetic aperture radar, polarimetry, change detection, copulas**

## I. Introduction

In remote sensing, synthetic aperture radar (SAR) offers numerous advantages over other imaging modalities, such as electro-optical. SAR is capable of penetrating clouds and can operate in both daytime and nighttime environments. This makes it suitable for persistent surveillance in commercial and military applications. SAR data has been exploited for a variety of tasks, including terrain segmentation, classification, and change detection. Many of these exploitation tasks have been performed using coherent, partially-coherent, non-coherent methodologies.

Recently, SAR sensors have become available that produce fully-polarimetric measurements [1]. These polarimetric SAR (polSAR) sensors transmit and receive in orthogonal polarizations, producing horizontal-horizontal (HH), vertical-vertical (VV), and cross-polarization horizontal-vertical (HV) measurements. The correlation between the backscatter measurements across the different polarization channels contains important information about materials within the scene. Accordingly, effective exploitation of polSAR data requires an accurate statistical model that captures both the per-channel marginal distributions as well as inter-channel correlation.

Financial support for S. H. was provided through the U.S. Air Force Civilian Academic Degree Program.

It is commonly assumed that the complex backscatter signal in each polarization channel follows a complex Gaussian distribution [2]. This is particularly true in low-resolution settings where large numbers of individual scatterers contribute to an aggregate response, and central limit theorem arguments prescribe a Gaussian distribution. In the Gaussian setting, existing polSAR change detection algorithms have been developed, either based directly on the Gaussian backscatter signal [3], [4], or on the corresponding Wishart-distributed polarimetric covariance matrix [5]. The Wishart change detection methodology is popular in SAR applications and represents a benchmark for change detection performance in the polSAR domain.

An opportunity exists to examine improvements to polSAR exploitation algorithms in high resolution scenarios where the Gaussian assumption breaks down. In this paper, we introduce a new model for polSAR data, combining generalized Gamma ($G\Gamma$) marginals with a copula-based multivariate dependency structure between polarization channels. The $G\Gamma$ distribution captures as special cases many non-Gaussian distributions applicable to single-channel backscatter magnitude, including the Weibull, Gamma, log-Normal, and Rayleigh distributions [6]. Therefore, the proposed copula-based multi-channel extension provides a flexible modeling framework for polSAR data and the change detection application considered in this paper.

In Section II, we present a brief motivation for polarization channel dependence modeling in polSAR and describe existing benchmark approaches. In Section III, we develop the $G\Gamma$-copula distribution and formulate an associated change detection algorithm based on the generalized likelihood ratio test. Finally, in Section IV, we present results from measured polSAR data showing advantageous performance under various scenarios against competing approaches.

## II. Background

### A. Polarimetric SAR Background

Recent SAR platforms are capable of fully-polarized measurements in which the radar system is able to transmit signals from two orthogonal polarizations and receive from orthogonal polarizations. These radars are able to measure the backscattering cross section of targets as a function of polarization. For a fully-polarimetric SAR system, after image

formation, the target vector $\boldsymbol{x}$ for each pixel is a complex $3\times 1$ vector representing the backscatter signal across each of the polarization channels,

$$\boldsymbol{x} = [x_{HH}, x_{HV}, x_{VV}]^T. \tag{1}$$

Because significant information exists in the relative behavior between polSAR channels, the polarimetric covariance matrix $\boldsymbol{\Sigma} = E[\boldsymbol{x}\boldsymbol{x}^H]$ is frequently considered as a polSAR data product from which exploitation can proceed. For example, in terrain classification [1], [7], it is common to explore decompositions of $\boldsymbol{\Sigma}$ based on either model-based approaches derived from volumetric models of electromagnetic scattering, or statistical approaches involving eigen-analysis of $\boldsymbol{\Sigma}$.

From measured data, $\boldsymbol{\Sigma}$ may be estimated using the sample covariance matrix,

$$\hat{\boldsymbol{\Sigma}} = \frac{1}{N}\sum_{i=1}^{N} \boldsymbol{x}_i \boldsymbol{x}_i^H, \tag{2}$$

where $\boldsymbol{x}_1, \ldots, \boldsymbol{x}_N$ is a collection of pixels from a region of interest. As noted earlier, low-resolution environments typically contain many scatterers per resolution cell resulting in an approximately Gaussian backscatter signal. In this case, the sample covariance matrix (2) follows a complex Wishart distribution. Specifically, when $\boldsymbol{x} \sim \mathcal{CN}(0, \Sigma)$ is a multivariate complex Gaussian distribution, then $N\hat{\boldsymbol{\Sigma}} \sim W_c(3, N, \boldsymbol{\Sigma})$, where the complex Wishart probability density function (PDF) is

$$p_{CW}(\boldsymbol{C}; p, N, \boldsymbol{\Sigma}) = \frac{1}{\Gamma_p(N)} \frac{1}{|\boldsymbol{\Sigma}|^N} |\boldsymbol{C}|^{N-p} e^{-tr[\boldsymbol{\Sigma}^{-1}\boldsymbol{C}]}, \tag{3}$$

and $\Gamma_p(N) = \pi^{p(p-1)/2} \prod_{j=1}^{p} \Gamma(N-j+1)$ [5].

The following section describes how this fact has been utilized for change detection in polSAR.

### B. Polarimetric change detection

In imagery analysis, it is often necessary to locate changes in images collected at two or more times. Performed manually by humans, this task is tedious has has a high probability of error. Automated algorithms can highlight these change regions to cue a human analyst or automated processing, such as classification. Seminal polSAR change detection work considers sample covariance matrices $\hat{\boldsymbol{\Sigma}}_1$ and $\hat{\boldsymbol{\Sigma}}_2$, respectively from Time-1 and Time-2, and treats change detection between the measurement times as a hypothesis test; under the no-change hypothesis $\mathcal{H}_0 : \hat{\boldsymbol{\Sigma}}_1 = \hat{\boldsymbol{\Sigma}}_2$, and under the change hypothesis $\mathcal{H}_1 : \hat{\boldsymbol{\Sigma}}_1 \neq \hat{\boldsymbol{\Sigma}}_2$.

The Wishart change detection algorithm [5] assumes Gaussian-distributed backscatter pixel vectors and formulates the hypothesis test as a generalized likelihood ratio test (GLRT) using the complex Wishart distribution (3) and sample covariance matrices. Assuming a region (or small block) of interest with $N$ co-registered pixels at each observation time, let $\boldsymbol{X}_1 = [\boldsymbol{x}_1, \ldots, \boldsymbol{x}_N]$ denote the pixels from Time-1; $\boldsymbol{X}_2 = [\boldsymbol{x}_{N+1}, \ldots, \boldsymbol{x}_{2N}]$ denote the pixels from Time-2; and the combined data be $\boldsymbol{X}_{12}$. Note that each column of $\boldsymbol{X}_1$, $\boldsymbol{X}_2$, and $\boldsymbol{X}_{12}$ corresponds to the backscattered signal given in (1). Then if matrix $\boldsymbol{C}_1 = \boldsymbol{X}_1\boldsymbol{X}_1^H$, $\boldsymbol{C}_2 = \boldsymbol{X}_2\boldsymbol{X}_2^H$, and $\boldsymbol{C}_{12} = \boldsymbol{X}_{12}\boldsymbol{X}_{12}^H$, the resulting GLRT detection statistic is

$$\begin{aligned} L(\boldsymbol{X_1}, \boldsymbol{X_2}) = &- 6N\log 2 - N\log|\boldsymbol{C}_1| \\ &- N\log|\boldsymbol{C}_2| + 2N\log|\boldsymbol{C}_{12}|. \end{aligned} \tag{4}$$

Note that $\boldsymbol{C}_1$, $\boldsymbol{C}_2$, and $\boldsymbol{C}_{12}$ must be positive definite, placing a lower bound on the number of samples $N$ used to estimate them. It can be shown that the algorithm in (4) is identical to the non-coherent polarimetric algorithm found in [3]; another commonly-referenced change detection approach.

The Wishart detector considers differences in cross-channel correlation structure. However, it is predicated on the Gaussian backscatter assumption. In Figure 1, we examine the distribution of measured high resolution SAR data provided by the AFRL Change Detection (CD) dataset from an X-band system with 0.25 m slant range resolution [8]. For the outlined region of interest, the lower left subfigure illustrates a histogram of pixel magnitudes from the HH channel ($|x_{HH}|$) along with maximum likelihood fits to several distributions. If vector $\boldsymbol{x}$ is complex Normal, then the magnitude $|\boldsymbol{x}|$ has a Rayleigh distribution. Hence, assessing the goodness-of-fit of the Rayleigh PDF to the magnitude histogram equivalently assesses the Gaussianity of the complex backscatter signal. However, the Rayleigh distribution shows clear limitations relative to the Weibull and $G\Gamma$ distributions—with the later qualitatively superior.

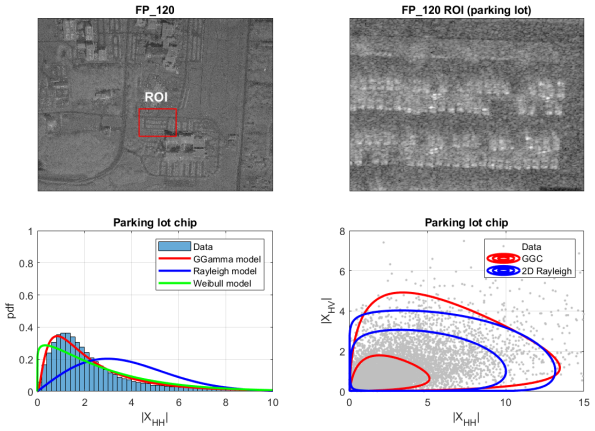


Fig. 1. Comparison of distributions used in SAR data modeling. Top-left: SAR map from which the chip was drawn. The parking lot region of interest (ROI) is enclosed by a red box. Top-right: zoomed-in chip over the ROI. Bottom-left: Data histogram over the $|X_{HH}|$ channel along with maximum likelihood fits for three distributions. Bottom-right: comparison $|X_{HH}|$ and $|X_{HV}|$ data with $G\Gamma C$ distribution and multivariate Rayleigh.

## III. Algorithm Description

### A. Rationale

The example in Figure 1, and numerous other proposed statistical models for SAR data [10] [11], illustrate the inadequacy of the Gaussian distribution. Hence, to fully exploit

polSAR data for change detection in a high resolution setting, a new multidimensional statistical model is needed.

Motivated by its generality, the single variate $G\Gamma$ distribution introduced by Stacy [12] was selected to model per-channel marginals because it captures as special cases many commonly used single-channel distributions for SAR data modeling, including the Weibull, Gamma, log-Normal, and Rayleigh, among others [6]. It has been applied in numerous settings, including single-channel and multi-channel SAR [13]. However, while the $G\Gamma$ distribution models the marginal distribution of individual polSAR channels more effectively than the Normal distribution (e.g., Fig. 1), it lacks a multivariate generalization required to jointly model multiple polarimetric channels. In this paper we employ the copula framework to create a multivariate extension of the $G\Gamma$ distribution and subsequently use that distribution to perform change detection.

### B. Statistical Model

The statistical model in this work is comprised of two components: the per-channel $G\Gamma$ marginal and a copula function modeling inter-channel correlation. For the magnitude $|x|$ of a particular polSAR channel, the $G\Gamma$ PDF is

$$p_{G\Gamma}(|x|; v, k, s) = \frac{v}{s\Gamma(k)} \left( \frac{|x|}{s} \right)^{kv-1} e^{-\left(\frac{|x|}{s}\right)^v}, \quad (5)$$

where $v, k, s > 0$ are parameters. The corresponding cumulative distribution function (CDF) is

$$F_{G\Gamma}(|x|; v, k, s) = \frac{\Gamma_z(k)}{\Gamma(k)}, \; z = (|x|/s)^v, \quad (6)$$

where $\Gamma_z(k)$ is the lower incomplete Gamma function. The one-dimensional $G\Gamma$ distribution plotted in Figure 1 comes from (5) after a maximum likelihood fit of the $(v, k, s)$ parameters.

With marginals in hand, we now turn our attention to inter-channel correlation, where we employ a copula framework. According to *Sklar's theorem*, any multivariate distribution may be written as a product of its marginals and a copula function [14]. Thus, using this framework, we are free to select marginal distributions most appropriate for polSAR data while separately capturing correlation with a copula function.

Formally, any CDF $F(x_1, x_2, \ldots, x_N)$ may be written $Q(F_1(x_1), F_2(x_2), \ldots, F_N(x_N))$, where for continuous random variables, $Q(\,)$ is a unique copula distribution, and each $F_i(x_i)$ is the marginal CDF for variate $x_i$. The probability density function corresponding to $F(\,)$ may be written

$$\begin{aligned} p\left(x_1, x_2, ..., x_N\right) =& q\left(F_1\left(x_1\right), F_2\left(x_2\right), \ldots, F_P\left(x_N\right)\right) \\ & p_1\left(x_1\right) p_2\left(x_2\right), \ldots, p_N\left(X_N\right), \end{aligned} \quad (7)$$

where $p_i(\,)$ is the marginal PDF corresponding to $F_i(\,)$, and $q(\,)$ is known as the *copula density*, obtained by differentiation of $Q(\,)$ [14].

Just as there are many choices for marginal distributions, there are many choices for copulas for modeling the dependence between marginals. In this work, we utilize the Gaussian copula density given as

$$q\left(u_1, u_2, ..., u_N\right) = \frac{1}{|\boldsymbol{\Lambda}|^{1/2}} \exp\left(-\boldsymbol{y}\left(\boldsymbol{\Lambda}^{-1} - I^N\right)\boldsymbol{y}^T\right), \quad (8)$$

where $\boldsymbol{y} = \left[\phi^{-1}\left(u_1\right), \phi^{-1}\left(u_2\right), ..., \phi^{-1}\left(u_N\right)\right]$, $\phi(\,)$ is the scalar standard Normal CDF, $\boldsymbol{I}_N$ is the $N \times N$ identity matrix, and $\boldsymbol{\Lambda}$ is a correlation matrix among the $N$ variates.

Letting $C = \{HH, HV, VV\}$ represent the set of channels in a fully polarmetric SAR system, we utilize (7) to form an $N = |C| = 3$ dimensional density over pixel magnitudes

$$p_{G\Gamma C}(|\boldsymbol{x}|; \boldsymbol{\theta}) = \prod_{c \in C} p_{G\Gamma}(|x_c|; v_c, k_c, s_c) q(u_{HH}, u_{HV}, u_{VV}), \quad (9)$$

where $u_c = F_{G\Gamma}(|x_c|; v_c, k_c, s_c)$ for each channel $c \in C$, and the magnitude $|\boldsymbol{x}|$ is taken element-wise. In (9), we refer to the copula-based multivariate extension of the $G\Gamma$ distribution as $G\Gamma C$. The distribution requires three parameters for the marginal of each channel, and three inter-channel correlation parameters, $\boldsymbol{\theta}_\rho = \{\rho_{HH,HV}, \rho_{HH,VV}, \rho_{HV,VV}\}$ that make up $\boldsymbol{\Lambda}$. All 12 parameters are collected into a parameter set $\boldsymbol{\theta} = \{(v_c, k_c, s_c) : c \in C\} \cup \boldsymbol{\theta}_\rho$.

In the lower right of Figure 1, we present example multichannel data from the X-band AFRL CD dataset [8] that bolsters support for the $G\Gamma C$ distribution over the typical Gaussian model for polSAR data. To highlight correlation between channels, the figure presents a $|x_{HV}|$ vs. $|x_{HH}|$ scatter plot of pixel magnitudes for a region of interest in the measured scene. Additionally, -1.5 dB and -3.0 dB probability density contours are shown for optimally fitted $G\Gamma C$ and Rayleigh distributions. The 2D Rayleigh distribution is chosen for comparison because the magnitudes of complex Gaussian random variables are Rayleigh distributed. Compared to the multivariate Rayleigh, we qualitatively observe that the $G\Gamma C$ model better captures the shape of the empirical multichannel data. In the following sections, we quantify the difference through improvement in change detection performance when the $G\Gamma C$ model is applied.

### C. Change Detection

The change detection algorithm is implemented as a hypothesis test, where under the no-change hypothesis, all pixel magnitudes are assumed to have the same distribution $\mathcal{H}_0 : \boldsymbol{X}_{12} \sim p_{12}$, and under the change hypothesis, Time-1 and Time-2 pixel magnitudes are drawn from unique distributions $\mathcal{H}_1 : \boldsymbol{X}_1 \sim p_1$, and $\boldsymbol{X}_2 \sim p_2$. Using the pixel set definitions of $\boldsymbol{X}_1$, $\boldsymbol{X}_2$, and $\boldsymbol{X}_{12}$ defined in Section II-B, and the previously developed $G\Gamma C$ distribution (9), the likelihood ratio is formed as

$$\begin{aligned} L(\boldsymbol{X}_1, \boldsymbol{X}_2) &= \frac{p(X_{12}|\mathcal{H}_1)}{p(X_{12}|\mathcal{H}_0)} \\ &= \frac{\prod_{i=1}^{N} p_{G\Gamma C}(|\boldsymbol{x}_i|; \boldsymbol{\theta}_1) \prod_{i=N+1}^{2N} p_{G\Gamma C}(|\boldsymbol{x}_i|; \boldsymbol{\theta}_2)}{\prod_{i=1}^{2N} p_{G\Gamma C}(|\boldsymbol{x}_i|; \boldsymbol{\theta}_{12})}. \end{aligned} \quad (10)$$

For a given threshold $\tau$, we choose $\mathcal{H}_1$ when $L(\boldsymbol{X}_1, \boldsymbol{X}_2) > \tau$, and $\mathcal{H}_0$ otherwise.

In (10), the parameters of the $G\Gamma C$ distributions are unknown. Consequently (10) is treated as a GLRT where maximum likelihood estimates (MLEs) of the parameters are used in place of unknown true values [9]. Time-1 data $\boldsymbol{X}_1$ is used to produce estimate $\hat{\boldsymbol{\theta}}_1$ of $\boldsymbol{\theta}_1$, and similarly estimates $\hat{\boldsymbol{\theta}}_2$ and $\hat{\boldsymbol{\theta}}_{12}$ are computed from sets $\boldsymbol{X}_2$ and $\boldsymbol{X}_{12}$, respectively. In this work, numerical optimization was used to maximize (9) when computing the MLEs.

Similar to other SAR CD algorithms, when performing CD over an entire image, an $M \times M$ block of pixels is taken around a particular pixel of test. The pixels in the block make up $\boldsymbol{X}_1$ and $\boldsymbol{X}_2$, and change detection is performed via (10). The process is repeated for all pixels of interest in the scene.

## IV. Results

To demonstrate the real-world performance of our G$\Gamma$C algorithm, we evaluated changes within an image chip of the AFRL CD dataset. For overall scene context, refer to Figure 1, where we have identified the region of interest as a parking lot. For this demonstration we focused on the FP_120 and FP_121 images. Unfortunately, ground-truth changes are not available for our dataset. To facilitate quantitative comparisons between the benchmark CD algorithms and the $G\Gamma C$ algorithm, known changes are introduced to small sections of the image that are otherwise unchanging. In the analyses to follow, we will compare the new $G\Gamma C$ change detection algorithm, denoted "copula", with the Wishart benchmark (Equation 4). We also make a second benchmark comparison using the single-channel non-coherent change detection algorithm from [3], denoted as "NCCD". For all complex vector pixels $\boldsymbol{x}$ given by (1), let $\boldsymbol{y} = |\boldsymbol{x}_{HH}| + |\boldsymbol{x}_{HV}| + |\boldsymbol{x}_{VV}|$ be the non-coherent combination of channels. The resulting scalar image is used in the NCCD algorithm given by

$$NCCD = 1 - \frac{\left(\frac{1}{N}\sum_{i=1}^{N}|\boldsymbol{y}_i|^2\right)\left(\frac{1}{N}\sum_{i=N+1}^{2N}|\boldsymbol{y}_i|^2\right)}{\left(\frac{1}{2}\left(\frac{1}{N}\sum_{i=1}^{N}|\boldsymbol{y}_i|^2 + \frac{1}{N}\sum_{i=N+1}^{2N}|\boldsymbol{y}_i|^2\right)\right)^2}. \tag{11}$$

We selected a 62×110 pixel area, shown in Figure 2, and then manipulated the images producing changes with high, medium, and low visual contrast. These cases are described below.

### A. Case 1: Moving a parked car into the road, high contrast

This case is shown in the left column of Figure 3. In this case, we selected a 10×10 pixel chip from Time-1 corresponding to a parked car. This chip was swapped with a 10×10 pixel chip from Time-2 corresponding to bare road surface, as indicated by the boxes and arrows. The Time-1 and Time-2 images confirm that this is a visually obvious change. We expect that this is a fairly straightforward change detection scenario. The ROC data in the bottom-left panel show that our assumption was correct, and all three algorithms perform well.

### B. Case 2: Moving a parked car into the road, medium contrast

This case is a variation on Case 1 with a parked car with a backscattered signal that appears less intense in magnitude with lower contrast in the measured SAR image. The Time-1 and Time-2 imagery, along with the ROC curve, are shown on the right column in figure 3. While the benchmark algorithms show a reduction in detection performance as a function of $p_{fa}$ the $G\Gamma C$ algorithm maintains approximately the same performance in Case 2 as Case 1.

### C. Case 3: Swapping bare roadway sections, low contrast

We wanted to experimentally establish a lower-bound on detection performance for all of the CD algorithms, including the $G\Gamma C$. So for Case 3, we selected a small section of bare road surface from Time-1 and swapped it with a section of bare road surface from Time-2. Note that the scattering phenomenology is very different in Case 3 than Case 1 and 2, as the road surface is homogeneous with no dominant scattering centers within the SAR resolution cell. This change has very low contrast. In such a case, the complex Gaussian model is representative of the scattering. The images and results for this case are found in the left column of figure 4. The Time-1 and Time-2 images highlight that this is a very difficult case, and one that cannot be performed visually. All three algorithms struggle with Case 3. Interestingly, the $G\Gamma C$ model is comparable with the Wishart model, whose physical interpretation is consistent with the scattering phenomenology.

### D. Case 4: Polarization shifting

In Case 4 we examine a change detection modality that is unique to polarimetric models. In this case, we circularly-shifted the polarization channel data for a single, car-sized chip from the parking lot image. In the Time-2 image, $\boldsymbol{X}_{HH} \rightarrow \boldsymbol{X}_{HV}$, $\boldsymbol{X}_{HV} \rightarrow \boldsymbol{X}_{VV}$, and $\boldsymbol{X}_{VV} \rightarrow \boldsymbol{X}_{HH}$. No changes were made to the Time-1 image. This type of change has physical meaning, as it may represent the rotation of a dominant, linearly-polarized scattering center relative to the SAR collection system. Images and ROC curve results are shown in the right column of Figure 4. The NCCD detector, which relies on the incoherent sum of polarization marginals, is blind to this type of change, while the Wishart and $G\Gamma C$ detectors are able to discern them. Among the polarimetric algorithms, $G\Gamma C$ appears to have superior detection performance.

## V. Conclusions

In this work, we show advantageous performance of a $G\Gamma C$ model for non-coherent change detection in polarimetric SAR. In particular, ROC analysis confirms that the $G\Gamma C$ model displays an ability to discriminate changes that is comparable or better than the benchmark NCCD and Wishart models. In the measured data analysis, for a $p_{fa} = 0.001$, $G\Gamma C$ detector has a $p_d$ that is 1.13 times higher than the Wishart detector in high contrast cases where the changes are visually discernible to 4.64 times higher in cases where

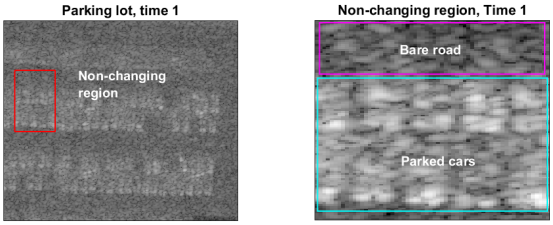


Fig. 2. Image chip from the AFRL CD dataset used in the demonstration. For display the image chips are incoherently summed across polarization channels. Left: full parking lot region of interest at Time-1 from FP_120. The non-changing section of the parking lot is highlighted with a red box. Right: non-changing region used in the induced changes study, a subset of the Time-1 data. Parked cars and bare road surface are highlighted in cyan and magenta, respectively.

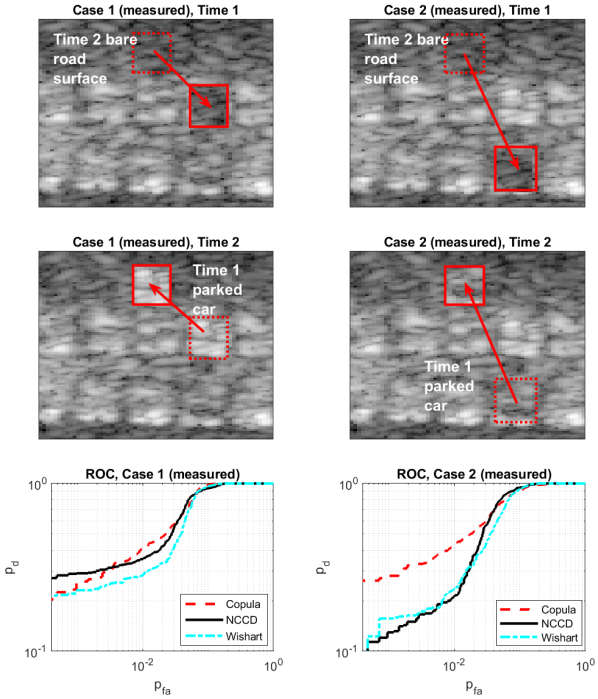


Fig. 3. Algorithm comparison using measured data from the AFRL CD challenge dataset. Ground-truth changes were created by translating image chips between the Time-1 and Time-2 images. Left column corresponds to Case 1 and right column corresponds to Case 2. Top row: Time-1 images. Second row: Time-2 images. While Case 1 shows visually apparent changes, the changes in Case 2 are more difficult to discern visually. Changes are indicated by the red boxes. Bottom row: ROC results. Analysis of these measured data shows that the $G\Gamma C$ model offers comparable or superior detection performance against the benchmarks in both visually obvious and visually challenging scenarios.

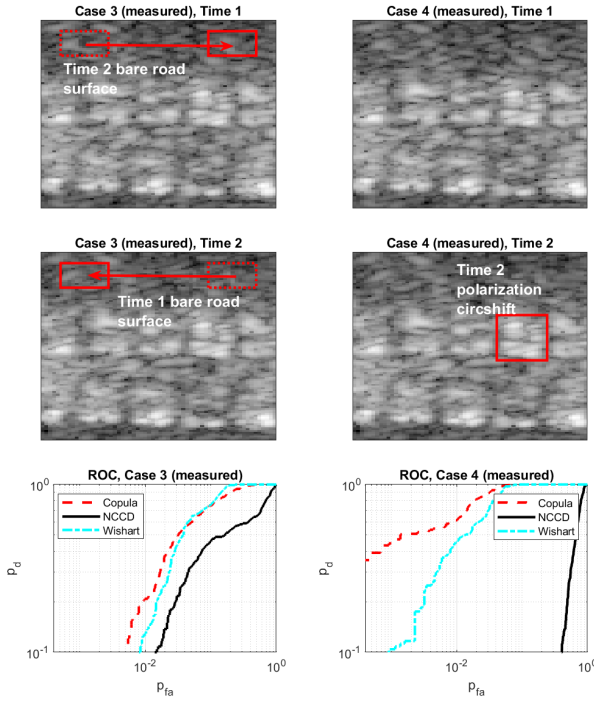


Fig. 4. Algorithm comparison using measured data from the AFRL CD challenge dataset. Ground-truth changes were created by translating image chips between the Time-1 and Time-2 images. Left column corresponds to Case 3 and right column corresponds to Case 4. Top row: Time-1 images. Second row: Time-2 images. Case 3 changes are impossible to discern visually, while the Case 4 changes are only visible through analysis of the polarization channel data. Changes are indicated by the red boxes. Bottom row: ROC results. Analysis of these measured data shows that the $G\Gamma C$ model offers comparable or superior detection performance against the benchmarks in both of these challenging scenarios.

changes are visually imperceptible. Using accurate marginals along with a capability to model cross-channel dependence, the $G\Gamma C$ model more efficiently exploits the data than existing benchmarks. The penalty of a more representative model is computational, as we need to resort to numerical methods to estimate the parameters of the $G\Gamma$ distribution. However, direct estimators for non-standard variations of the $G\Gamma$ distribution have been reported in the literature [15], and these will be explored for integration into the proposed CD framework.

While we have chosen the Gaussian copula there are many other choices of copula functions available. Each are likely to have different characteristics when applied to the real polSAR data [14]. For example, the Gaussian copula is limited to supporting linear dependence, whereas real polSAR data may include non-linear dependence. Other copula function are suitable for non-linear dependence. We plan to evaluate additional copula functions to understand the trade-space, as well as improve our parameter estimation procedure, in follow-on research.

## DISCLAIMER

The views and conclusions contained herein are those of the authors and should not be interpreted as necessarily repre-

senting the official policies or endorsements, either expressed or implied, of Air Force Research Laboratory (AFRL) or the U.S. Government.

## REFERENCES


[1] Eric Pottier, Jong-Sen Lee, Laurent Ferro-Famil "Advanced Concepts in Polarimetry - Part 1", NATO RTO-EN-SET-081, 2004.

[2] J. W. Goodman, "Some fundamental properties of speckle," J. Opt. Soc. Amer., vol. 66, no. 11, pp. 1145–1150, Nov. 1976.

[3] Leslie M. Novak "Change detection for multi-polarization, multi-pass SAR", Proceedings Volume 5808, Algorithms for Synthetic Aperture Radar Imagery XII, 2005.

[4] Joshua N. Ash, "Joint imaging and change detection for robust exploitation in interrupted SAR environments," Algoritms for Synthetic Aperture Radar XX, Proceedings of SPIE, May 2013.

[5] Knut Conradsen, Allan Aasbjerg Nielsen, Jesper Schou, Henning Skriver, "A Test Statistic in the Complex Wishart Distribution and Its Application to Change Detection in Polarimetric SAR Data, IEEE Transactions in Geoscience and Remote Sensing, Vol 41., No. 1., January 2003.

[6] E. W. Stacy, G. A. Mihram, "Parameter estimation for a Generalized Gamma Distribution," Technometrics, Vol. 7, No. 3, Aug. 1965.

[7] Motofumi Arii, "Retrieval of Soil Moisture Under Vegetation using Polarimetric Radar", PhD Dissertation, California Institute of Technology, 2009.

[8] Steven M. Scarborough, LeRoy Gorham, Michael J. Minardi, Uttam K. Majumder, Matthew G. Judge, Linda Moore, Leslie Novak, Steven Jaroszewksi, Laura Spoldi, and Alan Pieramico "A challenge problem for SAR change detection and data compression", Proc. SPIE 7699, Algorithms for Synthetic Aperture Radar Imagery XVII, 76990U, 18 April 2010

[9] Steven Kay, "Fundamentals of Statistical Signal Processing: Detection Theory", Volume 2, Prentice-Hall, 1998.

[10] Deng, Xinping, Carlos López-Martínez, Jinsong Chen, and Pengpeng Han, "Statistical Modeling of Polarimetric SAR Data: A Survey and Challenges" Remote Sensing Vol. 9, No. 4, 2017.

[11] Carlos Lopez-Martinez, Xavier Fabregas, "Polarimetric SAR Speckle Noise Model",IEEE Transactions on Geoscience and Remote Sensing, Vol 41, No 10, October 2003.

[12] E. W. Stacy, "A Generalization of the Gamma Distribution", The Annals of Mathematical Statistics, Vol. 33, No. 3, Sept. 1962.

[13] Heng-Chao Li, Vladimir A. Krylov, Ping-Zhi Fan, Josiane Zerubia, William J. Emery,"Unsupervised Learning of Generalized Gamma Mixture Model with Application in Statistical Modeling of High-Resolution SAR Images", IEEE Transactions on Geoscience and Remote Sensing, Vol. 54, No. 4, April 2016.

[14] Thorsten Schmidt, "Coping with copulas", Copulas-From Theory to Application in Finance, January 2007.

[15] Heng-Chao Li, Wen Hong, Yi-Rong Wu, Ping-Zhi Fan,"On the Empirical-Statistical Modeling of SAR Images With Generalized Gamma Distribution", IEEE Journal of Selected Topics in Signal Processing, Vol. 5, No. 3, June 2011.